

Development of Tide–Surge Interaction Model for the Coastal Region of Bangladesh

Gour Chandra Paul^{1,2} · Ahmad Izani Md. Ismail¹ · Azizur Rahman³ ·
Md. Fazlul Karim⁴ · Ashabul Hoque²

Received: 8 January 2014 / Revised: 9 May 2016 / Accepted: 11 May 2016 / Published online: 24 May 2016
© Coastal and Estuarine Research Federation 2016

Abstract In this paper, a two-dimensional, vertically integrated hydrodynamic model is developed taking into account entrained air bubbles during storm surges as well as incorporating inverted barometer, and river and land dynamics. The model is specifically designed for the coastal region of Bangladesh. A nested scheme method with a fine mesh scheme (FMS), capable of incorporating the complex coastline and all major offshore islands accurately, nested into a coarse mesh scheme (CMS) covering up to 15° N latitude in the Bay of Bengal is used. To incorporate the small and big offshore islands in the Meghna estuarine region with its complex coastline accurately, a very fine mesh scheme (VFMS) is again nested into the FMS. Along the northeast corner of the VFMS, the Meghna river discharge is taken into account. The coastal and island boundaries are approximated through proper stair steps. The model equations are solved by a semi-implicit finite difference technique using a staggered C-grid. A stable appropriate tidal condition over the model domain is generated by applying tidal forcing with the four major tidal constituents M_2 , S_2 , K_1 , and O_1 along the southern open

boundary of the CMS. This tidal regime is introduced as the initial state of the sea for nonlinear interaction of tide and surge. The model is applied to simulate water levels due to the interaction of tide and surge associated with the cyclones April 1991 and Aila at different coastal and island locations along the coast of Bangladesh. The results are found to be quite satisfactory with root mean square error of ~0.50 m as calculated for both the storm events. Tests of sensitivities on water levels are carried out for air bubbles, offshore islands, river discharge, inverse barometer, and grid resolution. The presence of air bubbles increases simulated water levels a little bit in our model, and the contribution of air bubbles in increasing water level is found around 2 %. Further, water levels are found to be influenced by offshore islands, river discharge, inverse barometer as well as grid resolution.

Keywords Hydrodynamic equations · Bay of Bengal · Surge · Air bubble · Tide · Nested schemes

Introduction

Granger and Smith (1995) defined storm tide phenomenon as the total water level attained by adding the height of the storm surge generated by a cyclone to that of the astronomical tide at the time the surge meets the coast. According to Smith (1989), storm surges kill globally, on average, 15,000 people a year. About 5 % of the global tropical cyclones and about 80 % of global casualties occur in the Bay of Bengal (see Debsarma 2009). The coastal belt of Bangladesh is especially vulnerable due to a complex coastline, thickly populated offshore islands of different shapes, shallow bathymetry, huge discharge through the Meghna and other rivers, high tidal range, etc. (Murty et al. 1986; Paul and Ismail 2013). Taking into account the reasons that affect surge along this area, an accurate

Communicated by Wayne S. Gardner

✉ Gour Chandra Paul
pcgour2001@yahoo.com

¹ School of Mathematical Sciences, Universiti Sains Malaysia, 11800 Pulau Pinang, Malaysia

² Department of Mathematics, University of Rajshahi, Rajshahi 6205, Bangladesh

³ Department of Computer Science and Engineering, University of Information Technology and Sciences, Rajshahi 6100, Bangladesh

⁴ Faculty of Engineering, Universiti Teknologi Brunei, Gadong, BE 1410, Brunei

prediction of water level is necessary for an effective early warning system and accurate flood risk estimation (e.g., Lewis et al. 2012, 2014).

The pioneering work of Das (1972) for the coast of Bangladesh was a linear stair step model used to simulate the surge caused by the November 1970 storm. In a linear stair step model, the total water level at a place is obtained by superimposing tide compiled from the tide table, if available, of the place with surge response obtained through a model simulation. Many analyses and predictions on storm surge, tide as well as their interaction for the head of the Bay of Bengal region have since then been advanced through the works of many investigators (see e.g., Johns and Ali 1980; Johns et al. 1985; Dube et al. 1985; Murty et al. 1986; Flather 1994; Roy 1995; Ali et al. 1997; As-Salek and Yasuda 2001; Dube et al. 2004; Paul and Ismail 2012a, b, 2013; Rahman et al. 2013). The first nonlinear tide surge interaction model due to Johns and Ali (1980) incorporated the influence of the Ganges–Brahmaputra–Meghna river system and offshore islands. The model due to Johns and Ali (1980) was a stair step model. It is to be noted here that in a stair step model, coastal and island boundaries are approximated along the nearest finite difference grid lines. Therefore, to represent the facts into account accurately in such a type of model, its grid resolution should be very high. But Johns and Ali (1980) conducted their study without ensuring an improved grid resolution, and therefore, the representations of coastal and island boundaries in the study were somewhat different from reality. Taking this fact into account, Roy (1995) developed the model of Johns and Ali (1980) by inserting a fine grid model for the Meghna estuarine area into a parental coarse grid model and tested the sensitivity of wind velocity and surge route on water levels due to the nonlinear interaction of tide surge. Simulated flood level was found to be highly sensitive to wind speed and cyclone landfall (see Johns and Ali 1980). Lewis et al. (2014) found this result for simulated inundation too. It is pertinent to note here that the study by Roy (1995) was included only two major offshore islands, Sandwip and Hatiya (Char Chenga). However, the coastal region of Bangladesh is populated with small and big islands (see Paul and Ismail 2012a), and offshore islands may influence surge levels (Roy 1999). However, it is a well-known phenomenon that during storm surges, wave breaking with extensive air bubble entrainment occurs in shallow water regions of a sea, and breaking waves disrupt the air–sea interface producing a two-phase layer, namely air bubbles in water and sea-spray droplets in air (see Soloviev and Lukas 2010). The spray and bubbles effectively increase the sea surface area so that the surface is no longer simply connected (Kraus and Businger 1994). These result in a mixed-phase environment that changes the dynamics as well as thermodynamics of the air–sea interaction (see Emanuel 2003;

Soloviev and Lukas 2010). The drag coefficient of wind stress at high wind speeds can be affected by ocean waves and the sea spray. The drag coefficient is usually important for extreme conditions with sea surface roughness, wind speed, and the stability of the atmosphere (see Pugh 1996; Moon et al. 2009; Zhihua et al. 2010). However, Hoque (2008), in a study of water level rise by entrained air in the surf zone, found a contribution of entrained air bubbles on wave set up in raising water level. Keeping the above facts in mind, Paul and Ismail (2012a) investigated storm surge problem along the coast of Bangladesh including entrained air bubbles and found their contribution on surge levels. The present work improves on that of Paul and Ismail (2012a), who derived a storm surge model to include air bubbles, and Paul and Ismail (2012b), who improved the model of Paul and Ismail (2012a) by interacting astronomical tide with surge nonlinearly. However, two important factors, namely river dynamics and inverse barometer, were not included in the model, and only major islands were taken into account via a stair step representation. It is mentioned earlier that the coast of Bangladesh is thickly populated with low lying small and big islands, and these islands as well as Meghna river discharge can influence surge levels along this region, especially along the Meghna estuarine area (Paul and Ismail 2013; Paul et al. 2014), wherein the inverse barometer may have a significant contribution. Therefore, for accurate prediction of peak water levels for the insufficiently studied region, all the factors that influence surge levels should properly be taken into account, which in turns can be important for estimating accurately coastal flood hazards (see Lewis et al. 2014). With the accurate estimation of water levels, a proper warning system can be developed, which can lead to guide evacuation of local population and rescue operations, and to develop a disaster management and vulnerability reduction action plan.

In this study, we develop the model of Paul and Ismail (2012b) for a more accurate prediction of water levels along the coast of Bangladesh and intend to see how our simulated results compare with observed and reported data. We also propose to show the effects of air bubbles, offshore islands, grid resolution, inverse barometer, and river discharge on water levels.

Methodology

Model Description

It is well-known that during stormy periods wave breaking with extensive air bubble entrainment occurs in shallow water

regions (see Chanson et al. 2006). Following Hoque and Aoki (2006), the water level rise Δh due to the entrained air bubbles above the still water depth h can be given by

$$\Delta h = \int_{-h-\Delta h}^0 C(z) dz, \quad (1)$$

where z is the vertical elevation positive upwards with $z=0$ at the mean surface and $C(z)$ represents the time averaged concentration and is given by

$$C(z) = C_0 \exp(k_1 z) \quad (2)$$

(see Hoque and Aoki 2005), which satisfies the boundary conditions

$$\left. \begin{array}{l} C(z) = C_0 \text{ at the surface } z = 0 \\ \text{and } C(z) \rightarrow 0 \text{ for } z \rightarrow -\infty \end{array} \right\} \quad (3)$$

Equation (1) on integration gives

$$\begin{aligned} \Delta h &= \frac{C_0}{k_1} [1 - \exp(-k_1 h - k_1 \Delta h)] \\ &= \frac{C_0}{k_1} \left[1 - \exp(-k_1 h) \left(1 - k_1 \Delta h + O((\Delta h)^2) \right) \right], \end{aligned}$$

which on simplification gives

$$\Delta h = \frac{C_0}{k_1} \frac{1 - e^{-k_1 h}}{1 - C_0 e^{-k_1 h}}. \quad (4)$$

In the above equations, C_0 indicates the reference void fraction at the mean water surface $z=0$, and k_1 is a decay parameter that characterizes vertical distribution of air bubbles.

As in Paul and Ismail (2012b), if the simplifications are made following Hoque and Aoki (2006) in averaged horizontal and vertical velocities, density, and pressure due to entrained air bubbles, we can write

$$\left. \begin{array}{l} u = u_w \\ v = v_w \\ w = w_w + C w_r \\ \rho = (1-C)\rho_w \\ p = p_w \end{array} \right\} \quad (5)$$

The subscript ‘ w ’ above refers to water, and w_r represents the rising velocity of an air bubble. It is to be noted here that the above assumptions do not satisfy the conservation of mass equation. The term $C(z)w_r$ is time-independent, which might be the reason of discontinuity (see e.g., Hoque and Aoki 2006). Now, to satisfy the continuity equation, we modify the term, following Hoque and Aoki (2006), as $w = w_w + w_c$, where w_c is a correction term. If the above simplifications are made, the hydrodynamic equations in a shallow coastal sea,

taking into account entrained air bubbles may be written as (see Paul and Ismail 2012b)

$$\frac{\partial u_w}{\partial x} + \frac{\partial v_w}{\partial y} + \frac{\partial w_w}{\partial z} = 0, \quad (6)$$

$$\begin{aligned} \frac{\partial u_w}{\partial t} + u_w \frac{\partial u_w}{\partial x} + v_w \frac{\partial u_w}{\partial y} + w_w \frac{\partial u_w}{\partial z} - f v_w \\ = -\frac{1}{\rho_w(1-C)} \left(\frac{\partial p_w}{\partial x} - \frac{\partial \tau_x}{\partial z} \right), \end{aligned} \quad (7)$$

$$\begin{aligned} \frac{\partial v_w}{\partial t} + u_w \frac{\partial v_w}{\partial x} + v_w \frac{\partial v_w}{\partial y} + w_w \frac{\partial v_w}{\partial z} + f u_w \\ = -\frac{1}{\rho_w(1-C)} \left(\frac{\partial p_w}{\partial y} - \frac{\partial \tau_y}{\partial z} \right), \end{aligned} \quad (8)$$

where the correction term w_c satisfies the equation

$$\frac{\partial w_c}{\partial z} - \frac{C_0 k_1 e^{k_1 z}}{1 - C_0 e^{k_1 z}} w_c = \frac{C_0 k_1 e^{k_1 z}}{1 - C_0 e^{k_1 z}} w_w, \quad (9)$$

which is subject to the condition that $w_c \rightarrow 0$ as $z \rightarrow -h$.

It is known that if the wavelength is large compared to the depth of water, the z -component of the momentum equation may be approximated by the hydrostatic equation, i.e.,

$$\frac{\partial p_w}{\partial z} = -\rho_w(1-C(z))g. \quad (10)$$

In the above equations, u_w , v_w , and w_w represent Reynolds averaged components of velocity in the directions of x , y , and z , respectively; f is the Coriolis parameter; g is the acceleration due to gravity; ρ_w is the density of the sea water; h is the sea depth from the mean sea level; p_w is the pressure at a point in the water; C_f represents the friction coefficient; and τ_x and τ_y are the components of Reynold’s stress.

Vertically Integrated Equations

A system of rectangular Cartesian coordinates is used for the derivation of vertically integrated equations, where the curvature of the Earth is assumed to be zero. The origin, O , of the system is set at the undisturbed level of the sea surface; OX and OY are directed towards the south and the east, respectively; and OZ is directed upwards. The displaced level of the free surface of the sea is given by $z = \zeta(x, y, t)$, and the position of the bed of the sea by $z = -h - \Delta h$ so that the total water column depth $H = h + \Delta h + \zeta$, where Δh is given by Eq. (4).

Let us denote the wind stress and bottom stress components by (T_x, T_y) and (F_x, F_y) , respectively, and the surface pressure

by P_a . Following Debsarma (2009), the bottom and surface conditions are given, respectively, by

$$(\tau_x, \tau_y) = (F_x, F_y) \text{ and } u_w = v_w = w_w = 0 \text{ at } z = -h(x, y) - \Delta h, \tag{11}$$

$$(\tau_x, \tau_y) = (T_x, T_y), P_w = P_a, \text{ and } w_w = \frac{\partial \zeta}{\partial t} + u_w \frac{\partial \zeta}{\partial x} + v_w \frac{\partial \zeta}{\partial y} \text{ at } z = \zeta. \tag{12}$$

If we integrate Eqs. (6)–(8) from $-h - \Delta h$ to ζ with the help of Eqs. (10)–(12) and if the simplifications following Paul and Ismail (2012a, b) are made, the vertically integrated shallow water equations in flux form can be given by (the subscript ‘w’ from u and v is dropped for convenience)

$$\frac{\partial \zeta}{\partial t} + \frac{\partial \tilde{u}}{\partial x} + \frac{\partial \tilde{v}}{\partial y} = 0, \tag{13}$$

$$\begin{aligned} \frac{\partial \tilde{u}}{\partial t} + \frac{\partial(\tilde{u}\tilde{u})}{\partial x} + \frac{\partial(\tilde{v}\tilde{u})}{\partial y} - f\tilde{v} = -gH \frac{\partial \zeta}{\partial x} \\ + B(h, \zeta, C_0) \left[\frac{1}{\rho_w} \frac{\partial p_a}{\partial x} + \frac{T_x}{\rho_w H} \frac{C_f \tilde{u}(u^2 + v^2)^{1/2}}{H^2} \right], \end{aligned} \tag{14}$$

$$\begin{aligned} \frac{\partial \tilde{v}}{\partial t} + \frac{\partial(\tilde{u}\tilde{v})}{\partial x} + \frac{\partial(\tilde{v}\tilde{v})}{\partial y} + f\tilde{u} = -gH \frac{\partial \zeta}{\partial y} \\ + B(h, \zeta, C_0) \left[\frac{1}{\rho_w} \frac{\partial p_a}{\partial y} + \frac{T_y}{\rho_w H} \frac{C_f \tilde{v}(u^2 + v^2)^{1/2}}{H^2} \right], \end{aligned} \tag{15}$$

where $(\tilde{u}, \tilde{v}) = H(u, v)$, u and v represent depth averaged components of velocity in the directions of x and y , respectively; $B(h, \zeta, C_0) = h + (1 + C_0)\zeta + \frac{2C_0}{k_1} \frac{1 - e^{-k_1 h}}{1 - C_0 e^{-k_1 h}}$; $\frac{\partial p_a}{\partial x}$ and $\frac{\partial p_a}{\partial y}$ are calculated following Vickery et al. (2000) from the relation $\frac{\partial p_a}{\partial r} = \frac{\Delta p_a H_0}{r_a} (R/r_a) \exp(-(R/r_a)^{H_0})$, where H_0 is the Holland’s radial pressure profile parameter wherein H_0 lies between 1 and 2.5 (see Holland 1980), Δp_a is the central pressure deficit, and descriptions about R and r_a will be found in “Wind Stress Generation” subsection.

Wind Stress Generation

For the generation of wind field in the region of interest, its wind information is needed. According to Paul and Ismail (2012a), the wind information in terms of the maximum sustained wind velocity and the corresponding radial distance from the eye of the storm and the difference of the atmospheric pressure between the eye and periphery can be obtained from the Bangladesh Meteorological Department (BMD). On the basis of the information, the wind field then can be generated by the use of various empirical formulae. For the Bay of Bengal region, a formula often used is due to Jelesnianski (1965) being given by

$$V_a = \begin{cases} V_0 \sqrt{(r_a/R)^3} & \text{for all } r_a \leq R \\ V_0 \sqrt{(R/r_a)} & \text{for all } r_a > R \end{cases}, \tag{16}$$

where V_0 is the maximum sustained wind at the maximum radial distance R and r_a is the distance between the cyclone center and the point at which the wind field is desired.

The wind stress can then be parameterized in terms of the wind field associated with the storm by the conventional quadratic law as (see Roy 1995)

$$(T_x, T_y) = \rho_a C_D (u_a^2 + v_a^2)^{1/2} (u_a, v_a), \tag{17}$$

where u_a and v_a stand for the x and y components of the surface wind, respectively; $\rho_a (= 0.00129 \times 10^3 \text{ kg m}^{-3})$ is the air density; and C_D is the surface drag coefficient. The drag coefficient C_D increases with wind speed, then levels off at high wind speeds (see e.g., Powell et al. 2003; Emanuel 2003; Moon et al. 2009). However, most modelers in storm surge modeling use a constant value of 2.8×10^{-3} for C_D throughout (Das 1994).

Boundary Conditions

The normal component of the depth averaged velocity at closed boundaries is set to zero, a condition of no flow across the model coastline and island boundaries. But, it cannot vanish at the open-sea boundary, and so, generally, radiation type of boundary condition is used to allow the disturbance, generated within the model area, to go out through the open boundary. Following Paul and Ismail (2012b), the western (85° E), eastern (95° E), and southern (15° N) open boundary conditions of the coarse mesh scheme are, respectively, given by

$$v + \left(\frac{g}{h + \Delta h} \right)^{1/2} \zeta = 0, \tag{18}$$

$$v - \left(\frac{g}{h + \Delta h} \right)^{1/2} \zeta = 0, \quad (19)$$

$$u - \left(\frac{g}{h + \Delta h} \right)^{1/2} \zeta = -2 \left(\frac{g}{h + \Delta h} \right)^{1/2} \sum_{i=1}^4 a_i \sin \left(\frac{2\pi t}{T_i} + \varphi_i \right), \quad (20)$$

where a_i , ϕ_i , and T_i are the amplitude, phase, and period, respectively, of the tidal constituent under consideration.

Numerical Aspects and Nested Grids

Set Up of Nested Schemes

In this study, the physical domain (referred to as coarse mesh scheme, CMS) covers the area between latitudes 15° N and 23° N, and longitudes 85° E and 95° E. To incorporate major offshore islands as well as complexities of the region of interest, a high-resolution numerical scheme (referred to as fine mesh scheme, FMS) covering the area between 21.25°–23° N and 89°–92° E is nested into the CMS. Again, considering the highly populated low lying small and big islands in the Meghna estuarine region and its complex coastline, a very fine mesh scheme (VFMS) covering the area between 21.77°–23° N and 90.40°–92° E is again nested into the FMS. It is of interest to note here that the whole coastal belt of Bangladesh is complex, but the Meghna estuarine area is especially complex, which is relatively flat and conducive to surge amplification (Ali and Choudhury 2014), and hence, VFMS is chosen for this region only. However, the regions for which the CMS, FMS, and VFMS are taken into account are shown in Fig. 1. Nested schemes are used in this study as they allow specification of high resolution in the area of importance only with lower resolution elsewhere. Such schemes can yield significant improvements in accuracy due to improved spatial resolution whilst reducing the number of computational grid points significantly and hence computational cost. The domains, grid resolutions, and number of computational grid points of our used schemes are shown in Table 1, while Fig. 2 depicts the used three schemes with grids as well as stair step representation of the coastal and island boundaries. The resolutions of grids employed in the FMS and VFMS can be able to solve the coastal and island complexities accurately (see Fig. 2). All the three schemes have the same hydrodynamic equations given by (13)–(15) but with different boundary conditions. Coupling of the schemes is important. The CMS is independent and is run, as we shall see later, with the boundary conditions prescribed by Eqs. (18)–(20), and the computed values of ζ , u , and v are passed along the open boundaries of the FMS in each time step of the solution process. It is pertinent to point out here that the grid resolutions of

the CMS and FMS are different. Therefore, the values of the parameters ζ , u , and v obtained from the CMS were interpolated using weighted interpolation to obtain a full set of boundary conditions for the FMS. In a similar way, the values of the parameters obtained from the FMS are supplied along the open boundaries of the VFMS for each time step of the solution process. Following Roy (1995), the Meghna river is considered between longitudes 90.4° and 90.6° E along the north east corner of the VFMS (see Fig. 1), and the discharge of the river is incorporated through

$$u_b = u + \frac{Q}{B(h + \zeta)}, \quad (21)$$

where Q and B are river discharge and breadth of the river, respectively. In our calculation, we have used $Q = 5100.0 \text{ m}^3/\text{s}$ (see Jain et al. 2007). It is known that there are more than 400 rivers in Bangladesh and all the rivers eventually discharge into the Bay either directly or indirectly (see Ali and Choudhury 2014). It is to be pointed out here that the Ganges–Brahmaputra–Meghna river system is the largest river system in Bangladesh and third largest freshwater outlet to the world's oceans (Milliman 1991). Thus, the fresh water discharges through other rivers are not as significant as that of the River Meghna, whose estuary is our region of concern, and hence, river discharge through the river Meghna is only considered.

The Data Sources and Used Numerical Values

The input data in the study are meteorological, oceanographical, hydrological, and geographical. Besides, the study involves a lot of parameters. The choices of their values are discussed before, and some of them are discussed in this subsection, and the rest of all have been assumed to have their standard values. The required meteorological inputs, namely storm path, central pressures, maximum sustained wind speed, and the radius of the maximum wind, were obtained from the BMD; later, they will be seen in “Model Experiments” subsection in details. The wind distribution of the study was generated based on the information available at the BMD with the use of the empirical-based formula due to Jelesnianski (1965). The study needs two geometrical factors, namely, coastal geometry and islands. The map of the study area was made with Google My Maps through ArcGIS software with which the three schemes, namely CMS, FMS, and VFMS, were created and were digitized according to their resolutions through a MATLAB routine, where the coastal and island boundaries were approximated through stair step algorithm using a MATLAB routine. The water depth data for the grid points of the CMS, FMS, and VFMS for the area extending from 21.25°–23° N and 89°–92° E were compiled from the survey group of Land Reclamation Project (LRP) under

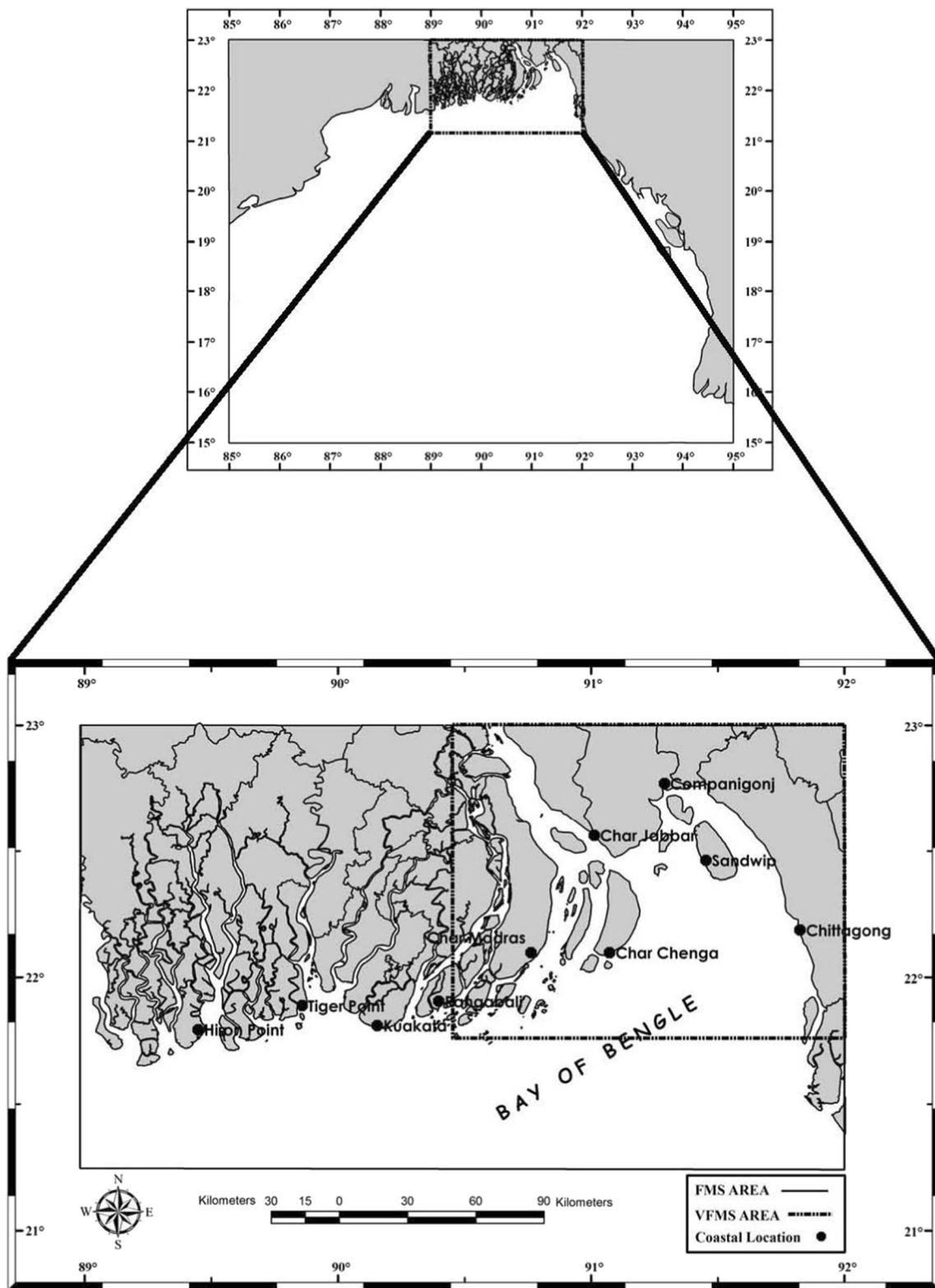


Fig. 1 Domains of the three schemes CMS, FMS, and VFMS and actual coastal and island boundaries along with ten representative locations at which computed results are presented

Bangladesh Water Development Board. Outside of the region, we took water depth data for some necessary grid points of the CMS from the figure quoted in Johns et al. (1985), and inverse

distance weighted interpolation was employed to interpolate the bottom for the other necessary grid points. Hydrological input, river discharge, was taken from the study of Jain et al.

Table 1 Domains, grid resolutions, and number of computational grids of different schemes

Scheme	Domain	Grid resolution along x axis	Grid resolution along y axis	Number of computational grids
CMS	15°–23° N and 85°–95° E	15.08 km	17.52 km	60 × 61
FMS	21.25°–23° N and 89°–92° E	2.15 km	3.29 km	92 × 95
VFMS	21.77°–23° N and 90.40°–92° E	684.70 m	808.03 m	200 × 205

(2007) as is aforementioned. The tidal data and observed water level data were collected from the Bangladesh Inland Water Transport Authority (BIWTA).

We have computed our results for $0 \leq C_0 \leq 0.7$, where our choice of $C_0 \leq 0.7$ is because it is the pseudo-free-surface threshold criterion (see Paul and Ismail 2012b). It is of interest to note here that in laboratory experiments, Hoque and Aoki (2006) found the value of C_0 as 0.3 for a plunging breaker and 0.2 for a spilling breaker, but according to them, the values may also depend on horizontal distance from breaking point.

The decay parameter k_1 for void fraction distribution in the surface zone was determined by fitting a theoretical curve to the experimental data. The value of k_1 was found to be 0.9 m^{-1} for the best fitted curve, and hence we used $k_1 = 0.9 \text{ m}^{-1}$. Even though we used a particular value for this parameter, the effects of its possible variations on water levels were also tested. The results with possible values of k_1 were found to be in general agreement with the ones presented in the study through graphical outputs in the respective cases. It is significant to point out here that some recent investigations are carried out applying wetting and drying scheme to include these effects (e.g., Madsen and Jakobsen 2004; Mashriqui et al. 2005). Since the highest resolution of the grids of the models used in the study is 0.6847 km (see Table 1), it cannot be capable of handling effectively the wetting and drying features in the area of interest. But, in order to prevent wet points from drying out, the water depth of a few points shallower than 3.0 m is artificially set to 3.0 m, which is taken based on the measured maximum tidal range (about 6.00 m) in the region of interest (see Barua 1997). A uniform value both for the friction and drag coefficients is used throughout the domain under consideration as $C_f = 0.0026$ and $C_D = 0.0028$, respectively (see Roy et al. 1999). The initial values of ζ , u , and v are taken as zero to represent an initial condition of static equilibrium (cold start). A time step of 60 s was used as such a value ensured the Courant–Friedrichs–Lewy (CFL) stability criterion.

Computational Procedure

The governing equations given by (13)–(15) as well as the boundary conditions given by (18)–(20) are discretized by a forward-time, central-space finite difference scheme with the use of the standard Arakawa C-grid, and the obtained

equations are solved by a conditionally stable semi-implicit method. The discretized equation obtained from Eq. (13) is firstly solved for ζ at the interior (even, odd) points of the CMS. Then, discretized boundary conditions are used to get ζ at the boundary (even, odd) points. After updating boundary points, average procedure is taken into account to get ζ at the remaining possible points, and finally, ζ is updated at the coastal and island boundaries. Then, after generating wind and pressure fields, the discretized equation obtained from Eq. (14) is solved for u evaluating the terms involved there by inserting the values of the necessary parameters, and finally, v is obtained in a similar fashion of u solving discretized equation obtained from Eq. (15). The parameters ζ , u , and v obtained in the CMS are supplied along the open boundaries of the FMS by the process discussed in “Set Up of Nested Schemes” subsection, and in a similar way, the results of the FMS were supplied along the boundaries of the VFMS to run it. Along the northern open segment of the VFMS, u_b is computed at points $(1, j)$ using Eq. (21), wherein u on the right hand side is replaced by $u_{3,j}$. This procedure is repeated over time supplying the updated values as initial conditions for calculating water levels due to tide, surge, and their interaction. It is pertinent to point out here that for generating a stable tidal regime, the model was run from the cold start in the absence of atmospheric pressure gradient force and wind stress taking $C_0 = 0$. The process of generation of stable tidal condition in the area of interest is discussed in “Generation of Tide over the Analysis Area” subsection. For the pure surge and total water levels due to the nonlinear interaction of tide and surge, the model is run for different choices of C_0 and with and without inclusion of inverse barometer, offshore islands, river discharge, and grid resolution. It is also to be noted here that for pure surge, the model was run from the cold start, and for total water levels due to tide–surge interaction, the generated pure tidal regime provided the initial condition at the model time $t = 0$.

Generation of Tide over the Analysis Area

The most energetic tidal constituent on the region under consideration is M_2 , the semidiurnal principal lunar tide (Paul and Ismail 2013), and some studies taking only the response to the M_2 tidal constituent are made along this region (Roy 1995, 1999; Paul and Ismail 2012b; Paul et al. 2014). This is, of

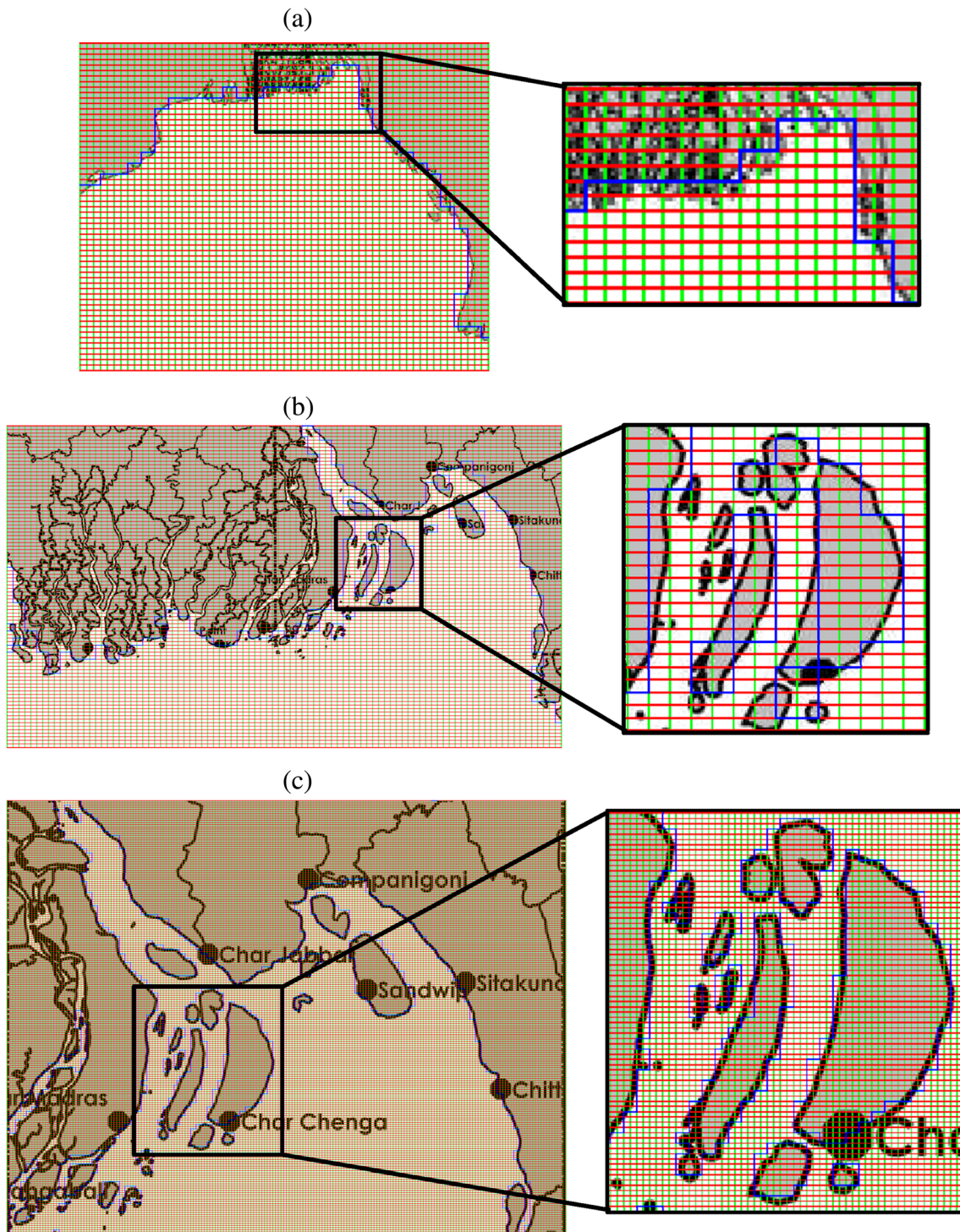


Fig. 2 Grids of the schemes CMS, FMS, and VFMS and approximated coastal and island boundaries though stair steps in the respective scheme with enlarged view at the right of each figure for the selected part; **a** CMS, **b** FMS, and **c** VFMS

course, a simplification, as there are strong spring/neap cycles in this area. Thus, to generate a proper tidal condition over the insufficiently studied region, tidal levels with the major tidal constituents, namely M_2 (principal lunar), S_2 (principal solar), O_1 (principal lunar diurnal), and K_1 (luni-solar diurnal), are taken at the

southern open boundary of the CMS, respectively, from part II, III, V, and IV of Schwiderski (1979, 1981a, b, c). A stable tidal regime over the model area is then generated from the cold start in the absence of atmospheric pressure gradient force and wind stress, and it is achieved after four tidal cycles of integration.

Model Experiments

The cyclones April 1991 and Aila that struck the coast of Bangladesh on 29 April 1991 and 25 May 2009, respectively, were taken into account to validate the simulations in comparison with observation, as we will see in the next section. The cyclone April 1991 was chosen because it passed nearby the Meghna mouth, the region of concern. On the other hand, we choose Aila, because it is the most recent severe cyclone for which more observations are available.

The Time History of the Cyclonic Storm April 1991

The cyclone was first detected as a depression on the 23rd of April in the satellite picture taken at the Space Research and Remote Sensing Organization (SPARRSO) from NOAA-I1 and GMS-4 satellites (see Khalil 1993). At 0300 universal time coordinated (UTC) of 25 April, the depression was located at 10.0° N latitude and 89.0° E longitude, which intensified into a deep depression at 1200 UTC near 11.5° N and 88.5° E and turned into a cyclonic storm at 1800 UTC near 11.5° N and 88.5° E of the same day with the maximum sustained wind 18–24 m s⁻¹, having a central pressure of 996 mb. The system retained this intensity until 0900 UTC of 27 April when it was found to have developed into severe cyclonic storm with the maximum wind speed 25–32 m s⁻¹, having 990 mb as the central pressure. On the same day at 1800 UTC, the system intensified into a severe cyclonic storm near 14.5° N and 87.5° E. It further intensified into a severe cyclonic storm with a hurricane core near 15.5° N and 87.5° E at 0300 UTC on April 28 that had wind speeds of more than 36 m s⁻¹. From about this time, it started moving in a north-

easterly direction towards the Meghna estuary and finally, crossed the Bangladesh coast a little north of Chittagong port at about 2000 UTC on April 29 (at about 0200 Bangladesh standard time on 30 April). The maximum wind speed observed at Sandwip was 65 m/s. The central pressure of the cyclone was as low as 938 mb, as measured by the Chittagong port authority of Bangladesh, and the estimated maximum pressure drop was about 60 mb (Talukder et al. 1992). Table 2 presents the time history of the great cyclone April 1991, and Fig. 3 displays the path of the cyclonic storm in the Bay of Bengal.

The Time History of the Cyclonic Storm Aila

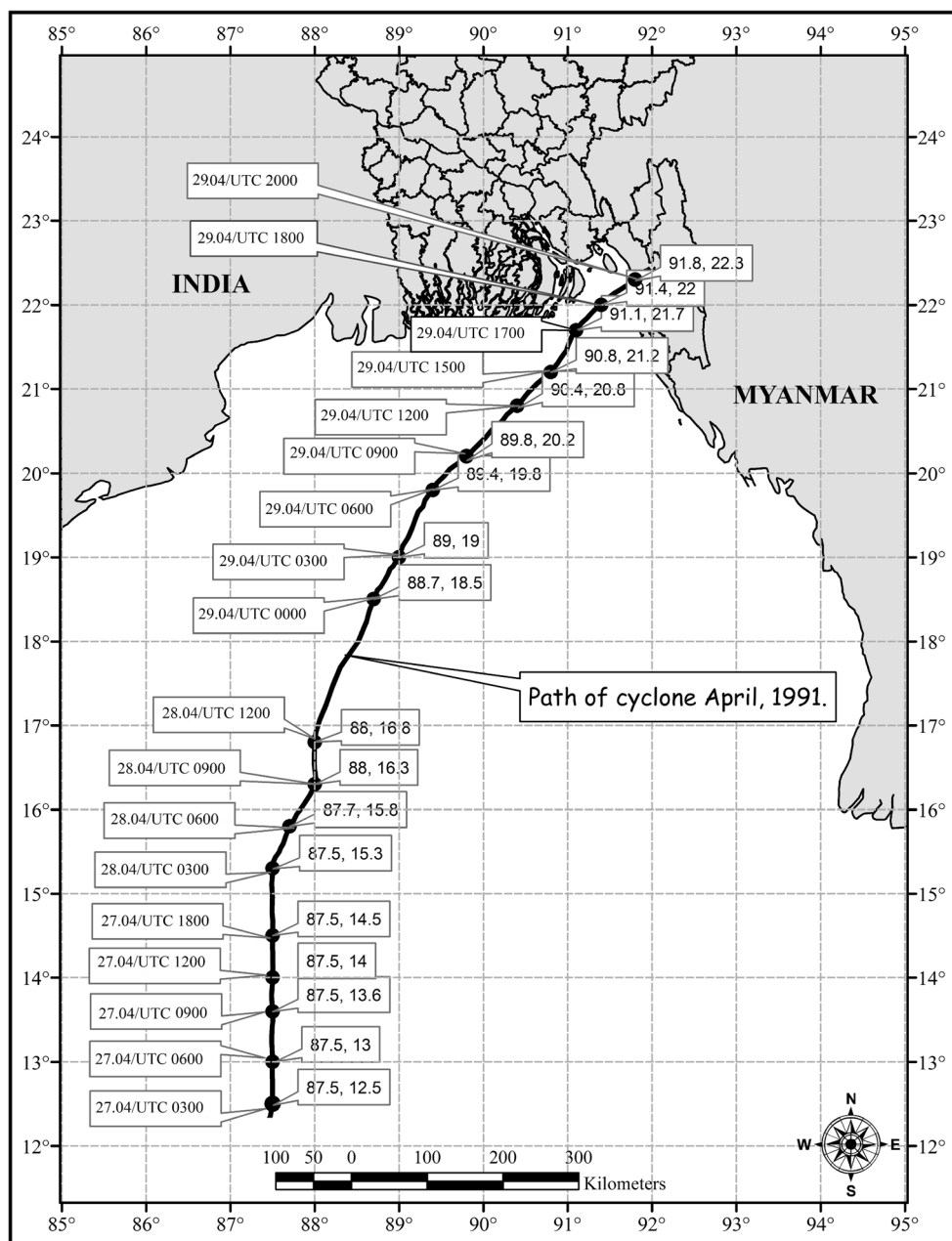
According to a report released by the BMD, a low formed over Southwest Bay and adjoining area at 0600 UTC of 21 May 2009. It moved northwards, and at 0300 UTC of 23 May, it intensified into a well-marked low over Southwest Bay and adjoining West Central Bay. At 0900 UTC of the same day, the system again intensified into a depression and moved northwards, and after 2100 UTC of the same day, it changed its direction and moved north-northeastwards and intensified further into a deep depression, which then developed into the cyclonic storm called Aila at 1200 UTC of 24 May, and about 0800 UTC of 25 May, the system started to cross West Bengal-Khulna in Bangladesh coast near Sagar island in India and then moved continuously northwards. At about 1200 UTC of May 25, the central position of the system positioned over Kolkata (India) and adjoining areas of India and Bangladesh but the remaining part of Aila was still crossing the coast. During the next 03–04 h, the system completed its crossing the coast and lay centered at West Bengal and

Table 2 Time series for the positions, central pressures, and the nature of the April 1991 cyclone (Source: BMD, Talukder et al. 1992)

Date (1991)	Hour (UTC)	Latitude (°N)	Longitude (°E)	Central pressure (mb)	Nature of the storm
26 April	1800	11.80	87.50	996.00	Cyclonic storm
27 April	0300	12.50	87.50	996.00	Cyclonic storm
27 April	0600	13.00	87.50	996.00	Cyclonic storm
27 April	0900	13.60	87.50	990.00	Severe cyclonic storm
27 April	1800	14.50	87.50	938.00	Severe cyclonic storm with hurricane core
28 April	0600	15.80	87.70	938.00	Severe cyclonic storm with hurricane core
28 April	0800	16.50	88.00	938.00	Severe cyclonic storm with hurricane core
28 April	1800	17.60	88.30	938.00	Severe cyclonic storm with hurricane core
29 April	0600	19.80	89.40	938.00	Severe cyclonic storm with hurricane core
29 April	1200	20.80	90.40	938.00	Severe cyclonic storm with hurricane core
29 April	1800	22.00	91.40	938.00	Severe cyclonic storm with hurricane core
29 April	2000	22.30	91.80	–	Crossing the coast near Chittagong
30 April	0000	23.00	92.40	–	Crossed the Bangladesh coast
30 April	0200	23.50	92.80	–	–

Maximum wind speed: 234 km h⁻¹, maximum radius of sustained wind: 50 km

Fig. 3 Track of the cyclone April 1991 (Data source: BMD)



adjoining western parts of Bangladesh. Table 3 presents the time history of the recent cyclone Aila, and the track of Aila with the available information from the BMD from 0600 UTC of 24 May 2009 is also plotted in Fig. 4.

Analysis of Results and Model Validation

The results for the storm April 1991 are computed for 80 h (from 1800 UTC of 26 April to 0200 UTC of 30 April), whereas those for the storm Aila 2009 are computed for 59 h (from 0900 UTC of 23 May to 2000 UTC of 25 May)

but for both the storm events, they are presented for the last 48 h at ten coastal and island locations of Bangladesh. The locations are Hiron Point, Tiger Point, Kuakata, Rangabali, Char Madras, Char Jabbar, Char Chenga, Companigonj, Sandwip, and Chittagong (Fig. 1). The obtained results of our computations are shown in diagrammatic forms through Figs. 5, 6, 7, 8, 9, 10, and 11 for some values of C_0 ($0 \leq C_0 \leq 0.7$). The diagrams for other values of C_0 are similar to the represented ones in each case, and hence, they have not been included. Thorough comparison of our computed time series of water levels to observation in most cases are restricted due to the unavailability of authentic observed time series data.

Table 3 Time series for the positions, central pressures, and the nature of the cyclone Aila over the Bay of Bengal during 23–26 May 2009 (Source: BMD)

Date	Hour (UTC)	Latitude (°N)	Longitude (°E)	Central pressure (mb)	Nature of the storm
23 May	0900	16.00	88.00	998	Depression
23 May	1500	16.50	88.00	996	Depression
24 May	0000	17.20	88.30	996	Depression
24 May	0600	17.80	88.60	994	Deep depression
24 May	0900	17.80	88.60	994	Deep depression
24 May	1200	18.30	88.60	994	Cyclonic storm
24 May	1800	18.80	88.60	990	Cyclonic storm
24 May	2100	19.20	88.60	987	Cyclonic storm
25 May	0000	19.40	88.60	987	Cyclonic storm
25 May	0300	20.00	88.60	987	Cyclonic storm
25 May	0600	21.60	88.30	987	Cyclonic storm
25 May	1200	22.90	88.30	970	Cyclonic storm
25 May	2000	24.20	88.50	980	Cyclonic storm

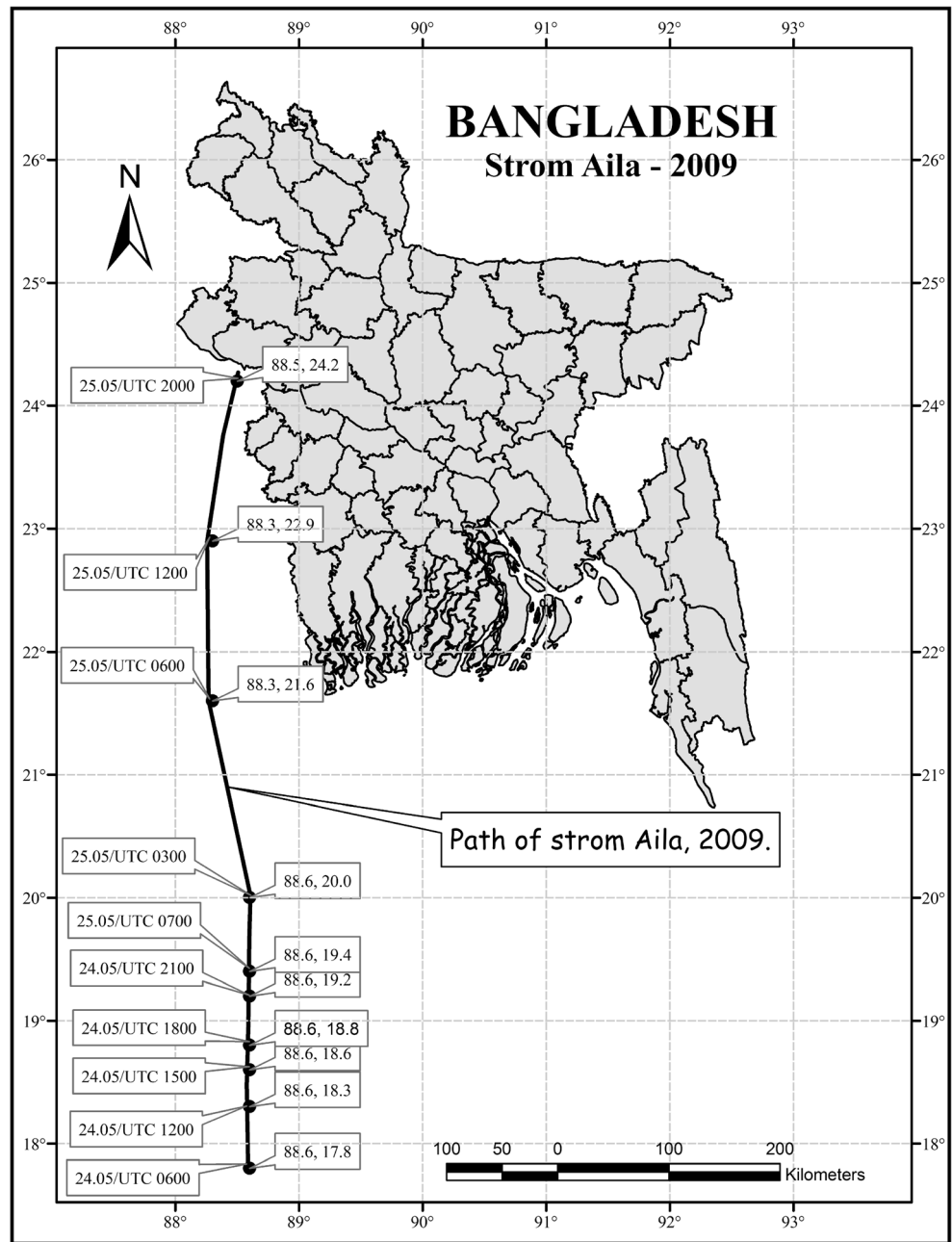
Maximum wind speed: 120 km h^{-1} , maximum radius of sustained wind: 54 km

Our computed time series of water levels due to surge associated with the storms April 1991 and Aila for $C_0=0.3$ at some coastal stations are depicted in Fig. 5. The maximum surge levels associated with the storm April 1991 resulted from our simulation for $C_0=0.3$ can be found to range from 2.96 to 7.65 m with 5.29 m at Chittagong (Fig. 5a), whereas without air bubbles ($C_0=0$), they can be found in the range of 2.91–7.15 m with 5.15 m at Chittagong (not shown). Roy et al. (1999) in their investigation found 0.70 (Hiron Point)–5.45 m high storm surge in the coastal areas of Bangladesh; Khalil (1993) reported 4–9 m high storm surge along these areas, whereas Paul and Ismail (2012b) simulated 2.69–6.98 m high surge. Thus our simulated water levels due to surge associated with the storm April 1991 compare well with the corresponding results obtained in different investigations mentioned above. But our computed surge levels at Hiron Point disagree with the result obtained in Roy et al. (1999). The reason behind it might be the approximation of the coastal geometry as we will see later. On the other hand, our computed maximum surge levels refer to the storm Aila for $C_0=0.3$ vary from 2.23 to 4.69 m with 2.88 m at Hiron Point (Sundarban, Khulna) (see Figs. 1 and 5b), whereas without air bubbles, the peak surge levels of 2.20–4.44 m are found with 2.84 m at Hiron Point (not shown). According to the Indian Meteorological Department (IMD), a storm surge of about 2–3 m above the astronomical tide was realized over coastal areas of West Bengal and adjoining Bangladesh coasts, and the maximum storm surge over Sundarban area was estimated to be about 2 m (Roy et al. 2009). Thus, our computed water levels due to surge associated with the storm Aila also fairly agree with some reported data.

Figure 6 depicts our model simulated water levels due to tide during the storm period for which the surge levels are presented for the cyclones April 1991 and Aila with the tidal data obtained from the BIWTA at Hiron Point and Chittagong. The choice of the two places is due to the availability of time series tidal data. Our computed tidal levels show reasonable agreement with the obtained data from the BIWTA (see Fig. 6).

Figure 7 shows our model simulated time series of water levels associated with both the considered storms due to tide, surge, their interaction, and superposition for the reference concentration $C_0=0.3$ at Hiron Point and Chittagong. It can be inferred from the figure that at the early stage, in both the storm events, tide dominates water levels but, after a certain length of time when the storm approaches the coast, the surge dominates water levels. These characteristics can be seen to be true for water levels at other locations. Other figures were omitted for sake of brevity. However, the water levels that came out through superposition of tide and surge compared well with the results obtained by the nonlinear interaction of tide and surge except at Chittagong for the storm Aila. It is of interest to note here that the astronomical tidal phenomenon is a continuous process in the sea, and so the surges due to tropical storms will always interact with the astronomical tide nonlinearly. Therefore, even though the superposition can yield similar results easily in comparison with those obtained from the nonlinear interaction of tide and surge, but it is far from reality, and hence, the rest of the results for total water levels are presented only for the interaction of tide and surge. The interaction effect (true water level minus surge minus tide) of tide and surge is also presented in each of the subplot of Fig. 7. It is seen from Fig. 7 that the interaction effect of tide

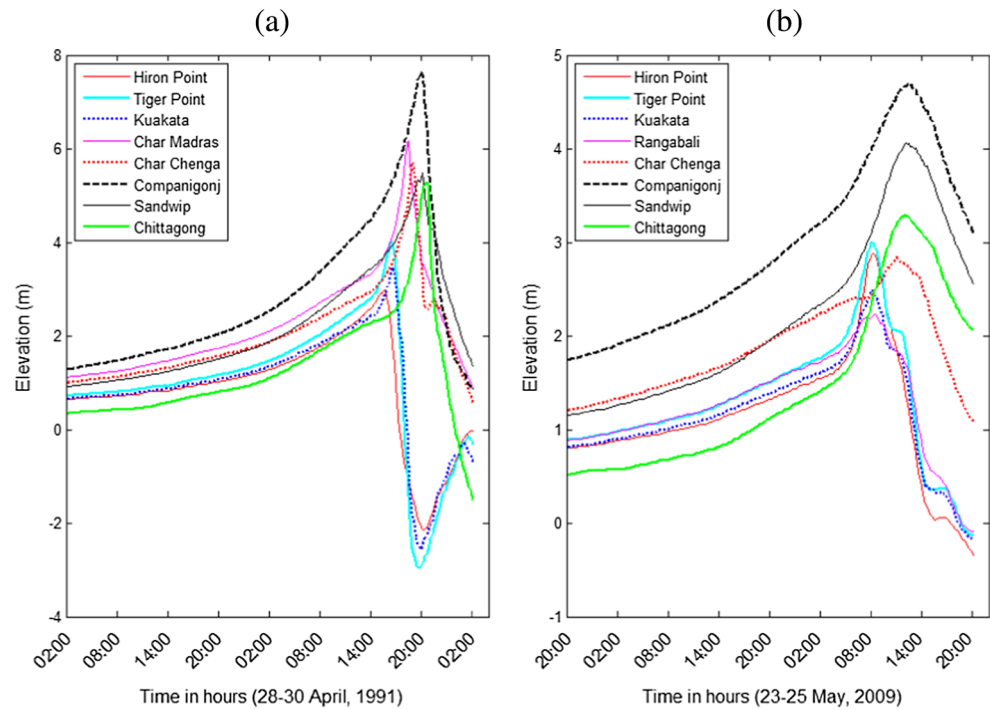
Fig. 4 Track of the cyclone Aila, 2009 (Data source: BMD)



and surge for the region of interest is non-negligible. It is also inferred from Fig. 7 that the interaction effect can affect the timing and extreme water levels during storm events. Thus, scientists and engineers need to understand the tide and surge interaction along the coast of Bangladesh in order to better estimates of extreme sea level in coastal defense. Our computed time series of total water levels associated with both the storms due to the interaction of tide and surge for $C_0=0.2$ at the remaining eight locations are shown in Fig. 8. The maximum total water levels with $C_0=0.2$, as simulated by the model, came out to be 3.32–7.26 m for the storm April 1991 (Fig. 8a, b), which is found to be in good agreement with the results obtained in Roy et al. (1999); Flather (1994); Paul and

Ismail (2012b, 2013), and Paul et al. (2014). On the other hand, the total water levels associated with the storm Aila were found to be 3.31–6.08 m (Fig. 8c, d). According to Roy et al. (2009), the overall water level associated with the storm Aila at the time of landfall was 4–5 m. Based on a report from the BMD, the storm Aila started to cross West Bengal Khulna coast near Sagar island in India nearly 0800 UTC of 25 May and made landfall between 0800 to 0900 UTC of 25 May over Bangladesh coast (Khulna) when the local astronomical tide was at peak. Our simulated results presented in Fig. 7c justify the landfall time of Aila at Hiron Point. Also by a report from the BMD, the central position of the system positioned over Kolkata (India) and adjoining areas of India

Fig. 5 Computed time series water levels with respect to the mean sea level due to surge associated with cyclones April 1991 and Aila at some coastal and island locations of Bangladesh for $C_0=0.3$; **a** for 1991 and **b** for 2009. These are results for the pure surge in the absence of tides



and Bangladesh at about 1200 UTC. Thus, our computed water levels associated with the storm Aila due to the interaction of tide and surge (see Figs. 7c, d and 8c, d) are also in good agreement with the sequence of events and data mentioned above. It can be inferred from Figs. 5, 7, and 8 that the peak water levels associated with both the storms due to surge and interaction of tide and surge at each location increase with time as the storm approaches the coast and finally, there is a recession. This is as to be expected because of increasing intensity of the wind while approaching the coast. The

beginning of recession of water levels at the western coastal stations occurs earlier than the ones at the eastern coastal stations. Early recessions of water levels for both the storms at the western costal locations are observed from the figures, which are as to be expected. A direct comparison of our time series elevation of sea surface with observed water levels for the chosen storms at Hiron Point, Char Chenga, and Chittagong is only made (see Fig. 9), where the data were obtained from the BIWTA. Our computed total water levels at these three stations compare well with observed ones for

Fig. 6 Comparison of our computed results ($C_0=0$) due to tide (with respect to the mean sea level) with the tidal data obtained from the BIWTA for the chosen periods of displaying results for the cyclones April 1991 and Aila at Hiron Point and Chittagong. In each case, a *dotted curve* represents the configuration for our computed tidal levels, and a *circle* represents an observed data; **a** at Hiron Point for April 1991, **b** at Chittagong for April 1991, **c** at Hiron Point for Aila, and **d** at Chittagong for Aila

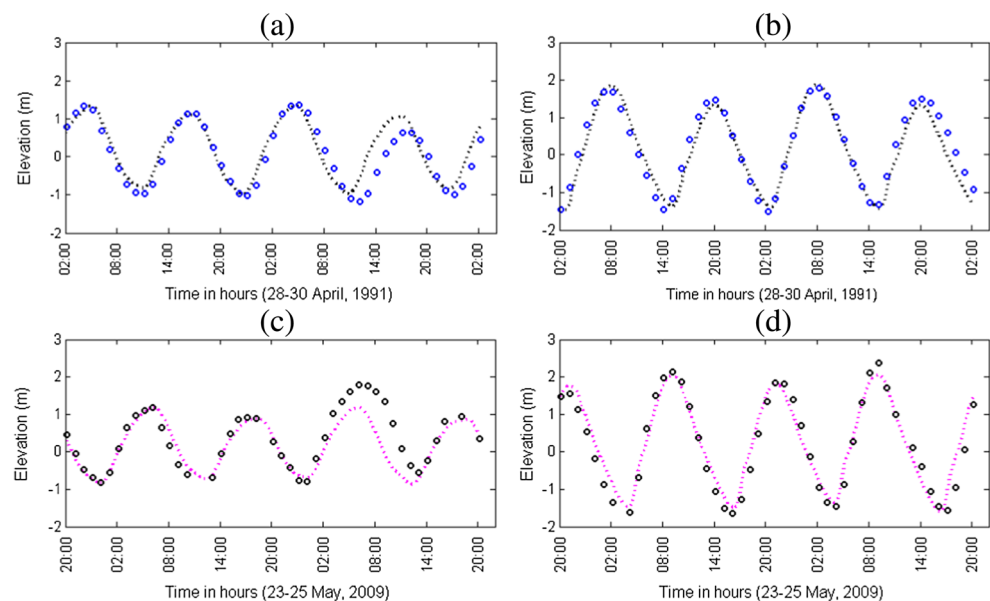
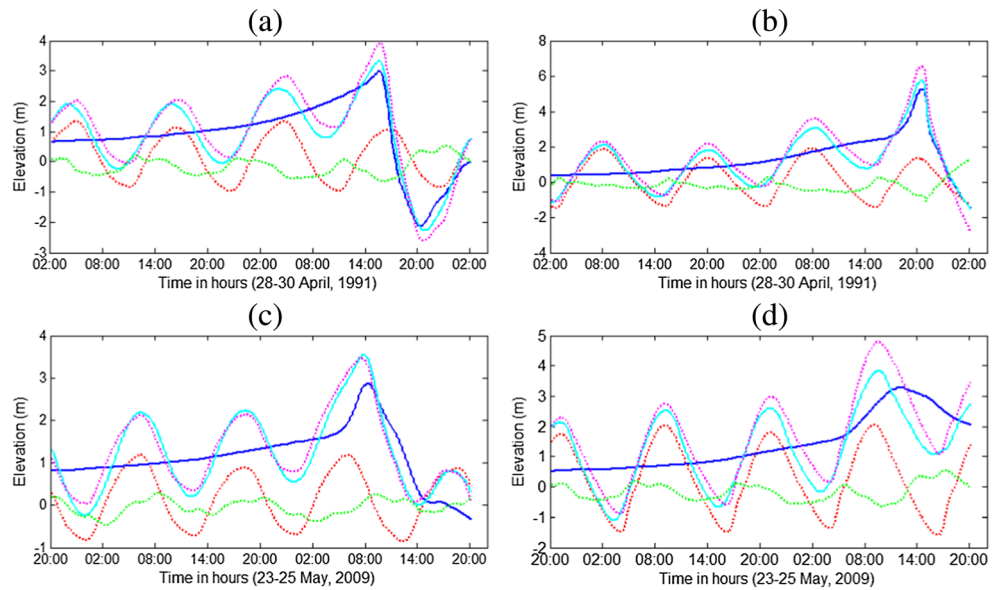


Fig. 7 Computed time series of total water levels ($C_0=0.3$) with respect to the mean sea level associated with the chosen storms at Hiron Point and Chittagong. In each case, a *dotted red curve* represents the configuration for tide, a *solid blue curve* for surge, a *solid cyan curve* for the interaction of tide and surge, a *dotted magenta curve* for superposition of tide and surge, and a *dotted green curve* for interaction effect; **a** at Hiron Point for April 1991, **b** at Chittagong for April 1991, **c** at Hiron Point for Aila, and **d** at Chittagong for Aila



both the storms. We could not compare our time series of total water levels at the remaining stations due to the lack of observed time series of water levels.

Tests of sensitivities were undertaken to investigate the effects of air bubbles, offshore islands, river discharge, grid resolution, and inverse barometer on water levels refer to the chosen storms. The changes in peak water levels (overall) with and without taking into account air bubbles for some values of the reference void fraction at our selected locations are shown in Fig. 10. It can be observed from the figure that the presence of air bubbles in our model increases water levels (up to ~9%), and it is also obvious from the figure that water level increases with the increasing reference void fraction, which is consistent with the results found in Paul and Ismail (2012a, b).

Further, it can be shown from the figure (Fig. 10) that the increase in water levels due to air bubbles depends on the levels of water also. Figure 11 delineates changes in peak water levels associated with the chosen storms for $C_0=0.2$ and without inclusion of each of the factors, namely air bubbles, offshore islands, river discharge, inverse barometer, and the VFMS, keeping the contributions of other factors unchanged. It is evident from the figure that the model simulates higher water levels in both the storm events along the Meghna estuarine area when river discharge is taken into account. Again, in the absence of offshore islands, peak water levels at each location along the Meghna estuarine area except at Char Madras and Char Jabbar can be shown to be increased from the figure, which is consistent with Roy (1999) except at

Fig. 8 Computed time series water levels with respect to the mean sea level due to the interaction of tide and surge associated with the storms April 1991 and Aila with $C_0=0.2$ at some stations along the coast of Bangladesh; **a** and **b** for April 1991, and **c** and **d** for Aila

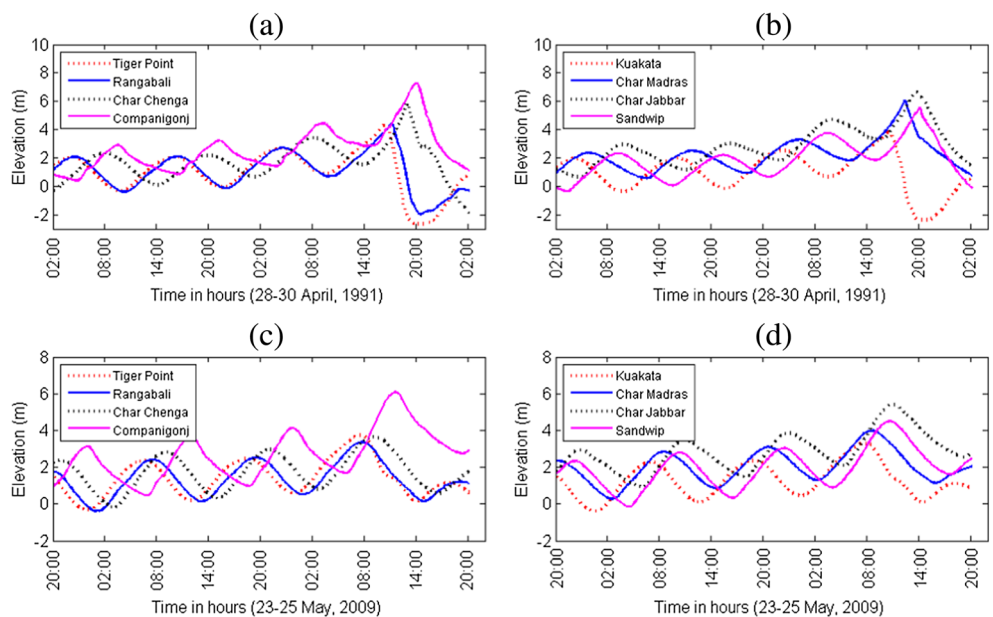
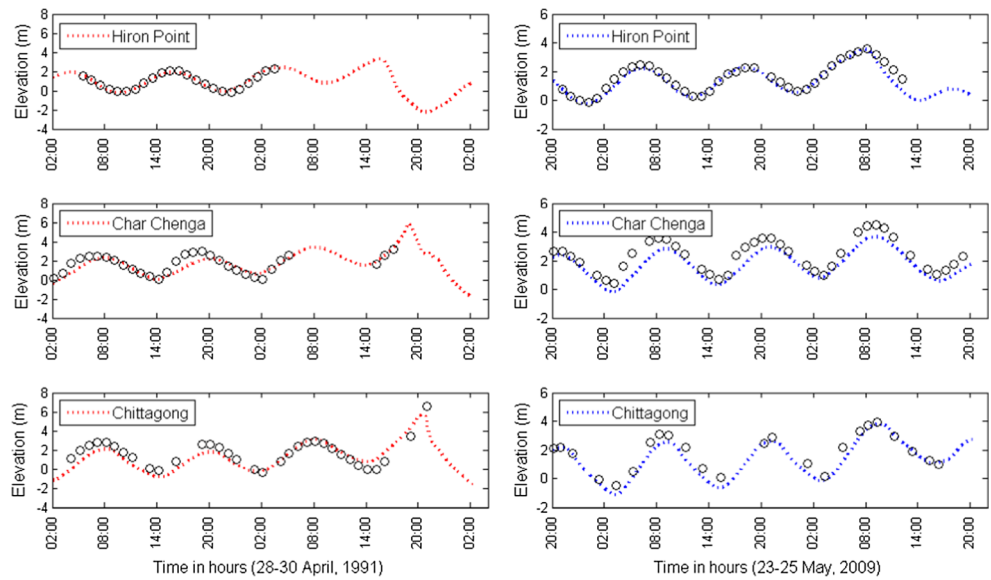


Fig. 9 Comparison of our simulated total water levels ($C_0 = 0.3$) with the observed data from the BIWTA at some stations refer to the storms April 1991 and Aila (the left panel for April 1991 and the right panel for Aila). In each case, a dotted curve represents the configuration for our computed time series of total water levels and a circle for that of observed one whenever available



Char Jabbar. It is to be noted here that the study due to Roy (1999) was conducted by including only the two major islands Sandwip and Hatiya (Char Chenga) along the Meghna estuarine area, and very fine grid resolution was not considered. But, grid resolution can affect surge intensity which can be seen to be true from Fig. 11. Thus, approximation of coastal geometry may be an exception in water levels at the location mentioned above. But, before making any final comments, more investigations are needed. Again, it can be inferred from Fig. 11 that the water levels for the region in close proximity to Hiron point are not affected by river discharge and offshore islands, which is as to be expected as the region is not so populated with islands as that of the Meghna estuarine area,

and the VFMS is not taken into account on this region. Further, it is inferred from Fig. 11 that the water levels refer to both the storms are greatly influenced by inverse barometer in comparison with the other factors involved in the study and the amount of sea surface elevation due to 1 mb drop in pressure can be found to result in about 1 cm (see Tables 2 and 3 and Fig. 11), which is consistent with the corresponding result found in Pugh (2004). It is of interest to note here that in shallow water, contribution from wind-stress forcing dominates that from the barometric forcing, and considering this fact, a large volume of works in the Bay of Bengal region is conducted neglecting the effect of inverse barometer (see e.g., Roy 1995; Roy et al. 1999; Dube et al. 2004; Debsarma 2009;

Fig. 10 Changes in peak water levels due to entrained air bubbles at some stations along the coast of Bangladesh with refer to the storms April 1991 and Aila; **a** for April 1991 and **b** for Aila

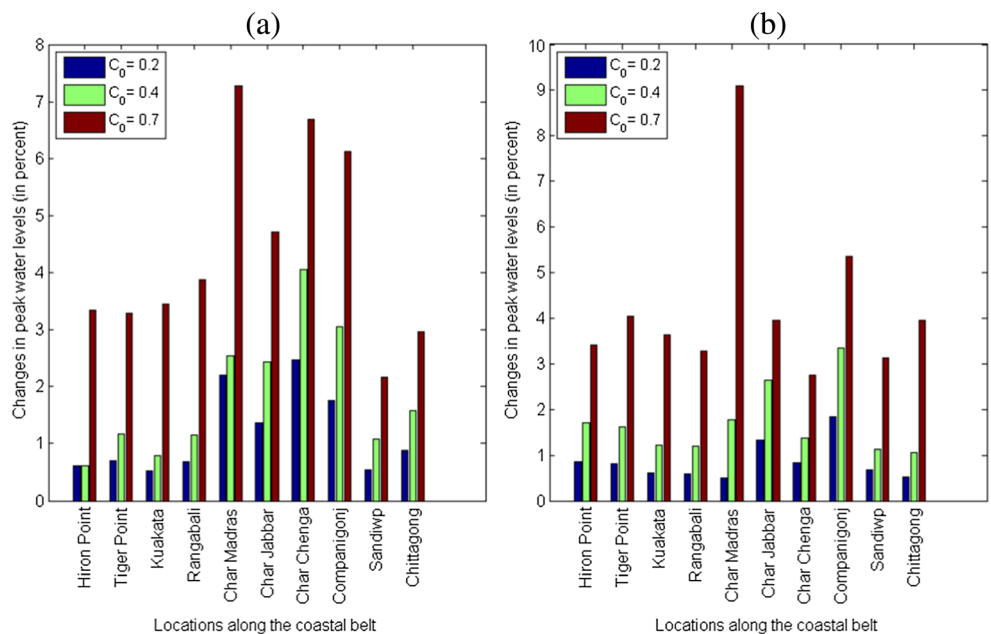
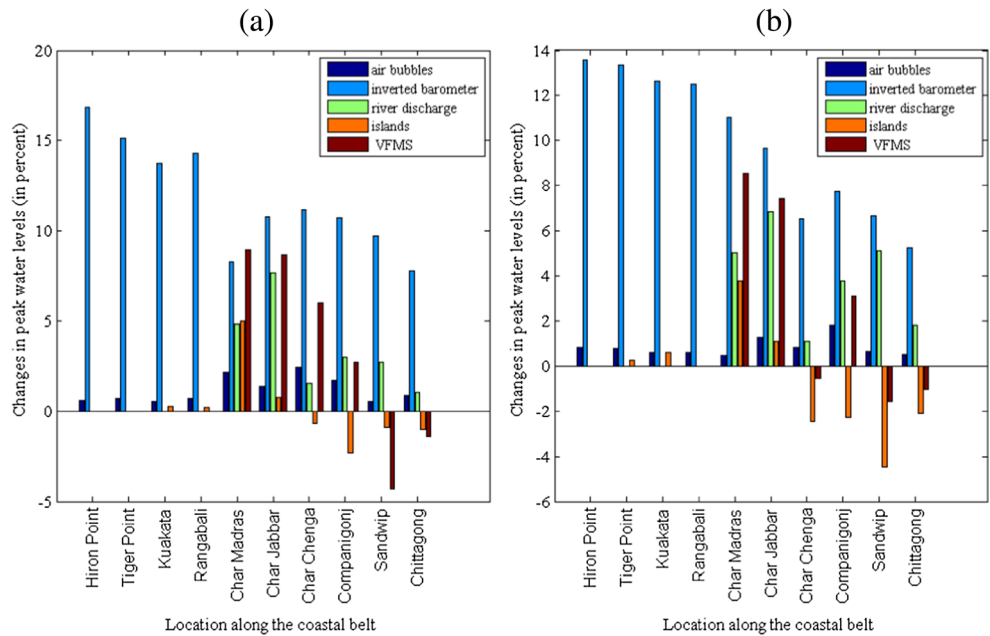


Fig. 11 Relative changes in peak water levels with respect to the run including the factors namely air bubbles with 20 % reference void fraction, inverted barometer, river discharge, islands, and VFMS and the runs without inclusion of each of the factors at some stations along the coast of Bangladesh with refer to the storms April 1991 and Aila; **a** for April 1991 and **b** for Aila



Paul and Ismail 2012b, 2013; Paul et al. 2014). But, the results as obtained by the study (see Fig. 11) due to the effect of inverse barometer suggest that the important factor in simulating water levels accurately due to a storm along the world most vulnerable region can never be neglected. Furthermore, it may be inferred from Fig. 11 that the effects of the factors mentioned above on water levels are great along the Meghna estuarine region, which may make the region the world most vulnerable one.

To test the performance of the model, the root mean square error (RMSE), a measure of accuracy, reliability for calibration and test datasets (Wösten et al. 1999), has been estimated between observed and computed overall water levels with $C_0=0.2$ referred to both the storms, where RMSE values are calculated with reference to observations and the mean is taken over several instants of time series data. Also, to show the relative importance of air bubbles, river discharge, offshore islands, inverted barometer, and grid resolution, the RMSEs

have also been evaluated. Our estimated RMSE values presented in Table 4 show that RMSE accuracy of our model for both the storm events is ~ 0.5 m, which in turn show a good agreement between observation and model results, where each of the factors, namely river discharge, inverse barometer, offshore islands, and grid resolution, has contribution (see Table 4 and Fig. 11) and that cannot be ignored. It may be mentioned here that Hiron Point is far away from the region where the VFMS and the offshore islands are implemented. Thus, the effect of offshore islands and VFMS might locally be bigger there than suggested in Table 4. Therefore, with the use of a very fine mesh scheme along the western coast, predictions might be improved there.

In our computations, we have used fixed value of the drag coefficient $C_D=0.0028$, the value most modelers use in storm surge modeling (Das 1994), where the values of C_D between 0.0025 and 0.003 are used (Mills, 1985) in some storm surge prediction models. Though we have used fixed value for C_D ,

Table 4 Estimated root mean square errors in meter. The errors have been estimated between computed and observed water levels in the last 48 h for each of the chosen storms (02.00 UTC of April 28 to 02.00 UTC of April 30 for the storm April 1991 and 20.00 UTC of May 23 to 20.00 UTC of May 25 for the storm Aila). We used almost all the data whenever available in the said period, where the observed data were received from

Storm	Costal station	Estimated by the model	Without air bubble	Without inverse barometer	Without river discharge	Without islands	Without VFMS	With $C_D=0.003$
April 1991	Chittagong	0.73	0.73	0.81	0.75	0.75	0.76	0.73
	Char Chenga	0.58	0.58	0.66	0.60	0.58	0.66	0.58
	Hiron Point	0.16	0.16	0.45	0.16	0.16	0.16	0.16
Aila	Chittagong	0.46	0.46	0.55	0.47	0.45	0.45	0.46
	Char Chenga	0.60	0.60	0.74	0.63	0.60	0.65	0.60
	Hiron Point	0.39	0.40	0.52	0.39	0.39	0.39	0.39

the BIWTA. In our calculation, we have used $C_D=0.0028$, the value most modelers use in storm surge modeling (DAS 1994). However, we have tested our results with the possible variation of C_D (0.0023–0.003) but test results only for $C_D=0.003$ are presented. The results for other values of C_D were found to be in general agreement with the results presented here

we have tested its possible variations (0.0025–0.003) on water levels and water levels are found to generally agree the results shown through graphical outputs of the study. RMSE values of our computed results with $C_D=0.003$ are presented in Table 4 for better understanding. It is to be noted here that the effect air bubbles on the drag coefficient is not taken into account. We also computed our results with the bathymetric data compiled and used by Roy (1995). The results in this case also generally agreed the graphical outputs presented in our study.

Uncertainty in simulated storm surge magnitude can arise from cyclone position, maximum sustained wind speed, and the radius of the maximum wind (Madsen and Jakobsen 2004; Lewis et al. 2014). Uncertainties in each of the parameters mentioned have been estimated with freely available data sources keeping the other parameters at a fixed value. The result in water level magnitude came out to be ~ 0.5 m, which is comparable to the water level prediction accuracy (see Table 4). It is to be noted here that uncertainties from freely data sources can be very high (Lewis et al. 2012).

A limitation of the study is the incorporation of a simple wetting and drying scheme, a proper treatment of the effect of the factor may be important in future work, but it is not possible to take care in the present model framework.

In this study, air bubbles seem to be of minor importance (see Fig. 10 and Table 4) despite being an upper limit estimation. It is of importance to note here that our predicted water levels before the storm can be slightly higher because of the artificial bubbles. But surge peak might not be affected significantly by this error. However, work still has to be done in order to take into account the horizontal distribution of air bubbles and the effect of bubbles on wind stress, which we are planning and the dependence of C_0 on wind speed may need to be included. Further improvement is being progressed by incorporating uncertainty in wind field assumptions from Holland (1980) taking into account a very fine mesh scheme along the whole coast of Bangladesh and will be reported in a future paper.

Conclusion

In this study, a model of cyclone-induced storm surge has been developed taking into account entrained air bubbles, inverted barometer as well as river and land dynamics. The developed model is applied to simulate water levels at some coastal and island locations of Bangladesh due to the interaction of tide and surge associated with the tropical storms April 1991 and Aila. In our model, higher water levels are simulated in the presence of air bubbles wherein much entrained air bubbles can be found to contribute more. The model-simulated results along the Meghna estuarine area are found higher when the river discharge is taken into account, and due to the existence

of offshore islands, the surge intensity is found to be influenced. Furthermore, water levels are found to be influenced with grid resolution and found to be increased greatly by inverted barometer in comparison with the other factors considered in this study. However, RMSE accuracy obtained in this study is ~ 0.5 m. Therefore, with the achieved RMSE accuracy, it is suggested that in order to obtain better predictions, one should ensure to have accurate meteorological data, inverse barometer effect, the river discharge, fine resolution of grids. In addition, one should ensure that the wind effect on the surge is modeled well.

Acknowledgments We would like to thank the five anonymous reviewers for their helpful comments and suggestions that helped improve the original manuscript. The first author expresses his grateful thanks to Government of Malaysia for offering financial grants during post-doctoral fellow scheme to Universiti Sains Malaysia, School of Mathematical Sciences, Pulau Pinang-11800, Malaysia. URL:<http://www.usm.my>. The authors are also thankful to Md. Mizanur Rahman, Assistant Professor, Department of Mathematics, Shahjalal University of Science and Technology, Sylhet, Bangladesh, and Mr. Md. Masum Murshed, and Md. Rabiul Haque, Assistant Professor, Department of Mathematics, University of Rashahi, Bangladesh, for providing necessary data and helpful discussion.

References

- Ali, A., and G.A. Choudhury. 2014. *Storm surges in Bangladesh: An introduction to CEGIS storm surge model*. Dhaka: The University Press Limited.
- Ali, A., H. Rahman, S. Sazzad, and S.S.H. Choudhary. 1997. River discharge, storm surges and tidal interaction in the Meghna River mouth in Bangladesh. *Mausam* 48: 531–540.
- As-Salek, J.A., and T. Yasuda. 2001. Tide–surge interaction in the Meghna estuary: Most severe conditions. *Journal of Physical Oceanography* 31: 3059–3072.
- Barua, D.K. 1997. The active delta of the Ganges-Brahmaputra Rivers: Dynamics of its present formations. *Marine Geodesy* 20: 1–12.
- Chanson, H., S. Aoki, and A. Hoque. 2006. Bubble entrainment and dispersion in plunging jet flows: Freshwater vs. seawater. *Journal of Coastal Research* 22: 664–677.
- Das, P.K. 1972. Prediction model for storm surges in the Bay of Bengal. *Nature* 239: 211–213.
- Das, P.K. 1994. On the prediction of storm surges. *Sadhana* 19: 583–595.
- Debsarma, S.K. 2009. Simulations of storm surges in the Bay of Bengal. *Marine Geodesy* 32: 178–198.
- Dube, S.K., P.C. Sinha, A.D. Rao, and G.S. Rao. 1985. Numerical modelling of storm surges in the Arabian Sea. *Applied Mathematical Modelling* 9: 289–294.
- Dube, S.K., P. Chittibabu, P.C. Sinha, and A.D. Rao. 2004. Numerical modelling of storm surge in the head Bay of Bengal using location specific model. *Natural Hazards* 31: 437–453.
- Emanuel, K.A. 2003. A similarity hypothesis for air–sea exchange at extreme wind speeds. *Journal of Atmospheric Sciences* 60: 1420–1428.
- Flather, R.A. 1994. A storm surge prediction model for the northern Bay of Bengal with application to the cyclone disaster in April 1991. *Journal of Physical Oceanography* 24: 172–190.

- Granger, K.J., and D.I. Smith. 1995. Storm tide impact and consequence modelling: Some preliminary observations. *Mathematical and Computer Modelling* 21: 15–21.
- Holland, G.J. 1980. An analytic model of the wind and pressure profiles in hurricanes. *Monthly Weather Review* 108: 1212–1218.
- Hoque, A. 2008. Studies of water level rise by entrained air in the surf zone. *Experimental Thermal and Fluid Science* 32: 973–979.
- Hoque, A., and S. Aoki. 2005. Distributions of void fraction under breaking waves in the surf zone. *Ocean Engineering* 32: 1829–1840.
- Hoque, A., and S. Aoki. 2006. Air entrainment by breaking waves: A theoretical study. *Indian Journal of Marine Sciences* 35: 17–73.
- Jain, S.K., P.K. Agarwal, and V.P. Singh. 2007. *Hydrology and water resources of India*, 308. Dordrecht: Springer.
- Jelesnianski, C.P. 1965. A numerical calculation of storm tides induced by a tropical storm impinging on a continental shelf. *Monthly Weather Review* 93: 343–358.
- Johns, B., and A. Ali. 1980. The numerical modeling of storm surges in the Bay of Bengal. *Quarterly Journal of the Royal Meteorological Society* 106: 1–18.
- Johns, B., A.D. Rao, S.K. Dube, and P.C. Sinha. 1985. Numerical modeling of tide-surge interaction in the Bay of Bengal. *Philosophical Transactions of the Royal Society A* 313: 507–535.
- Khalil, G.M. 1993. The catastrophic cyclone of April 1991: Its impact on the economy of Bangladesh. *Natural Hazards* 8: 263–281.
- Kraus, E.B., and J.A. Businger. 1994. *Atmosphere-ocean interaction*, second ed., Oxford University Press, pp. 362.
- Lewis, M., P. Bates, K. Horsburgh, J. Neal, and G. Schumann. 2012. A storm surge inundation model of the northern Bay of Bengal using publicly available data. *Quarterly Journal of the Royal Meteorological Society* 139: 358–369.
- Lewis, M., K. Horsburgh, and P. Bates. 2014. Bay of Bengal cyclone extreme water level estimate uncertainty. *Natural Hazards* 72: 983–996.
- Madsen, H., and F. Jakobsen. 2004. Cyclone induced storm surge and flood forecasting in the northern Bay of Bengal. *Coastal Engineering* 51: 277–296.
- Mashriqui, H.S., G.P. Kemp, I. van Heerden, J. Westerink, B. Ropers-Huilman, K. Strelva, A. Binselam, and Y.S. Seok. 2005. Bay of Bengal cyclone surge modeling program: Use of super computer technology and GIS for early warning, in 13th international conference on geoinformatics, August 17–19, 2005, Toronto, Canada.
- Milliman, J.D. 1991. Flux and fate of fluvial sediment and water in coastal seas. In *Ocean margin processes in global change*, ed. R.F.C. Mantoura, J.M. Martin, and R. Wollast, 69–89. Chichester: Wiley.
- Mills, D.A. 1985. A numerical hydrodynamic model applied to tidal dynamics in the Dampier Archipelago. Bulletin no. 190, Department of Conservation and Environment, Western Australia.
- Moon, I.-J., J.-I. Kwon, J.-C. Lee, J.-S. Shim, S.K. Kang, I.S. Oh, and S.J. Kwon. 2009. Effect of the surface wind stress parameterization on the storm surge modeling. *Ocean Modelling* 29: 115–127.
- Murty, T.S., R.A. Flather, and R.F. Henry. 1986. The storm surge problem in the Bay of Bengal. *Progress in Oceanography* 16: 195–233.
- Paul, G.C., and A.I.M. Ismail. 2012a. Numerical modeling of storm surges with air bubble effects along the coast of Bangladesh. *Ocean Engineering* 42: 188–194.
- Paul, G.C., and A.I.M. Ismail. 2012b. Tide-surge interaction model including air bubble effects for the coast of Bangladesh. *Journal of the Franklin Institute* 349: 2530–2546.
- Paul, G.C., and A.I.M. Ismail. 2013. Contribution of offshore islands in the prediction of water levels due to tide-surge interaction for the coastal region of Bangladesh. *Natural Hazards* 65: 13–25.
- Paul, G.C., A.I.M. Ismail, and M.F. Karim. 2014. Implementation of method of lines to predict water levels due to a storm along the coastal region of Bangladesh. *Journal of Oceanography* 70: 199–210.
- Powell, M.D., P.J. Vickery, and T.A. Reinhold. 2003. Reduced drag coefficient for high wind speeds in tropical cyclones. *Nature* 422: 279–283.
- Pugh, D.T. 1996. *Tides, surges and mean sea-level*. Chichester: Wiley.
- Pugh, D. 2004. *Changing sea levels: effects of tides, weather, and climate*. Cambridge University Press.
- Rahman, M.M., G.C. Paul, and A. Hoque. 2013. Nested numerical scheme in a polar coordinate shallow water model for the coast of Bangladesh. *Journal of Coastal Conservation* 17: 37–47.
- Roy, G.D. 1995. Estimation of expected maximum possible water level along the Meghna estuary using a tide and surge interaction model. *Environment International* 21: 671–677.
- Roy, G.D. 1999. Inclusion of off-shore islands in transformed coordinate shallow water model along the coast of Bangladesh. *Environment International* 25: 67–74.
- Roy, G.D., A.B.M.H. Kabir, M.M. Mandal, and M.Z. Haque. 1999. Polar coordinates shallow water storm surge model for the coast of Bangladesh. *Dynamics of Atmospheres and Oceans* 29: 397–413.
- Roy, K., U. Kumar, H. Mehedi, T. Sultana, and D.M. Ershad. 2009. *Initial damage assessment report of cyclone Aila with focus on Khulna District*, 14. Khulna: Unnayan Onneshan-Humanitywatch-Nijera Kori.
- Schwiderski, E.W. 1979. Global ocean tides, part II. Atlas of tidal charts and maps. Naval surface weapons center tech. Memo. NSWC/TR-79-414, 89.
- Schwiderski, E.W. 1981a. Global ocean tides, part III. Atlas of tidal charts and maps. Naval surface weapons center tech. Memo. NSWC/TR-81-122, 84 pp.
- Schwiderski, E.W. 1981b. Global ocean tides, part IV. Atlas of tidal charts and maps. Naval surface weapons center tech. Memo. NSWC/TR-81-142, 87 pp.
- Schwiderski, E.W. 1981c. Global ocean tides, part V. Atlas of tidal charts and maps. Naval surface weapons center tech. Memo. NSWC/TR-81-144, 85 pp.
- Smith, D.K. 1989. *Natural disaster reduction: How meteorological and hydrological services can help*, Publication No. 722. Geneva: World Meteorological Organisation.
- Soloviev, A., and R. Lukas. 2010. Effects of bubbles and sea spray on air-sea exchange in hurricane conditions. *Boundary-Layer Meteorology* 136: 365–376.
- Talukder, J., G.D. Roy, and M. Ahmed. 1992. *Living with cyclone*. Dhaka: Community Development Library.
- Vickery, P.J., P.F. Skerlj, A.C. Steckley, and L.A. Twisdale. 2000. Hurricane wind field model for use in hurricane simulations. *Journal of Structural Engineering* 126: 1203–1221.
- Wösten, J.H.M., A. Lilly, A. Nemes, and C. Le Bas. 1999. Development and use of a database of hydraulic properties of European soils. *Geoderma* 90: 169–185.
- Zhuhua, Z., Y. Wang, D. Yihong, C. Lianshou, and G. Zhiqiu. 2010. On sea surface roughness parameterization and its effect on tropical cyclone structure and intensity. *Advances in Atmospheric Sciences* 27: 337–355.